Small-Signal Model of Variable-Frequency Flyback Converter

Brian T. Irving, Yuri Panov, and Milan M. Jovanović
Power Electronics Laboratory
Delta Products Corporation
P.O. Box 12173, 5101 Davis Dr.
Research Triangle Park, NC 27709, USA
birving@deltartp.com

***Abstract*—An accurate, straight-forward, small-signal model of the variable-frequency flyback converter is presented. The model, which replaces the switching devices with dependent sources representing average terminal currents, is similar to the discontinuous-conduction-mode, three-terminal switch model presented in the past. However, since the converter always operates at the boundary of discontinuous and continuous-conduction-modes under both steady state and transient conditions, the inductor can be removed from the average large-signal model. In fact, the control-to-output transfer function can be accurately described with its current loop closed at frequencies less than half of the switching frequency. The model is extended to the ringing-choke converter, which is a common type of variable-frequency flyback converter used in many cost-sensitive applications. The small signal model is validated with measurements made on an offline, 5-V/ 2-A experimental prototype.**

Keywords- ringing-choke; RCC; small signal; DCM-CCM; boundary operation

I. INTRODUCTION

The variable frequency flyback converter has been used by industry for a wide range of applications for many years. It is attractive in low power applications because it is does not suffer from significant reverse-recovery-related losses of the output diodes, as does the constant frequency, continuous-current mode (CCM) flyback converter, while offering a lower peak input current, and hence, lower conduction losses, than the constant frequency, discontinuous-current mode (DCM) flyback converter. In cost-sensitive applications, the control circuit can be implemented discretely without the use of a control IC, often resulting in a very low component count.

Although the variable frequency flyback converter appears to be a simple circuit, the modeling of circuits dynamics is not well understood, and, consequently, control-loop compensation is often designed using a cut-and-try approach. The modeling approaches in the past [1] – [2] do not consider a variable frequency converter which operates at the boundary of DCM and CCM. Recently, a small-signal model of a variable-frequency flyback converter has been presented in [3] which was developed using state-space approach, and which suggests the presence of a right-half-plane (RHP) zero in the control to output transfer function of the power stage. Another model recently developed [4] also reports a RHP zero in the control to output transfer function. However, neither [3] nor [4] validate the existence of the RHP zero through measurements. Furthermore, it is shown from [3] that the minimum RHP zero frequency, which occurs with a duty cycle equal to one, is one third of the switching frequency, and increases beyond the switching frequency for duty cycles less than one-third (i.e., for $D<1/3$). The fact that the RHP zero appears at high frequency may be due to the closed current loop, as suggested by [5], which has the tendency to cause the RHP zero to "disappear". Since in many applications the RHP zero does not impact practical loop design, for simplicity sake, an argument can be made whether to include the inductor in the model at all!

In this paper, a straight-forward small-signal model of the variable-frequency flyback converter is presented which is shown to be accurate over a practical frequency range (i.e., up to one tenth of the switching frequency), despite the fact that a RHP zero is not present in the model. By neglecting the state of the inductor, the converter model with its current loop closed results in a lower order characteristic polynomial. This approach is also beneficial when considering an additional output filter stage, which tends to increase the order of the characteristic polynomial.

II. VARIABLE FREQUENCY FLYBACK CONVERTER

A simplified circuit diagram of the variable frequency flyback converter is shown in Fig. 1, whereas its key switching waveforms are shown in Fig. 2. Error voltage V_e, which is the amplified difference between output voltage V_O and reference voltage V_{REF} through error amplifier EA, is compared at the pulse width modulator (PWM) to sense voltage V_S, which is proportional to switch current i_{S1}. When the voltage at the positive input of the PWM exceeds its negative input, i.e., when $v_S > v_e$, the reset input of RS latch turns off main switch S_1. Conversely, when diode current i_d decreases to zero, zero-current-detect (ZCD) circuit initiates the turn on of main switch S_1 through the set input of RS latch. Generally, the circuit utilizes peak current mode control and operates at the boundary of CCM and DCM. It is, therefore, a variable switching frequency system, whose switching frequency varies as a function of input voltage and output load.

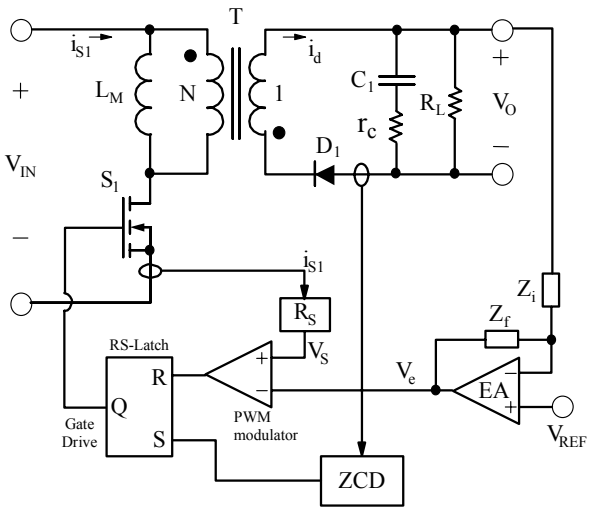

Figure 1. Functional circuit diagram of variable-frequency flyback converter.

From a modeling point of view, the flyback converter shown in Fig. 1 can be represented equivalently as a buck-boost converter by reflecting its primary side to its secondary side, as shown in Fig. 3(a). The three terminal PWM switch, which consists of switch S and diode D_1, is identified along with active, common, and passive terminals a, c, p, respectively, as discussed in [2]. Terminal current waveforms i_a, i_p, and i_c are also shown in Fig. 3(b), where active current i_a linearly increases during on time t_{ON} of switch S (i.e., during off time of diode D_1), passive current i_p, which is equal to diode current i_d, linearly decreases during off time t_{OFF} of switch S (i.e., during on time of diode D_1), and common current i_c is the sum of active and passive current i_a and i_p, respectively.

A. Average Large Signal Model

The average large-signal model of the buck-boost power stage can be obtained by replacing switch S with dependent current source I_a and diode D_1 with dependent current source I_p,

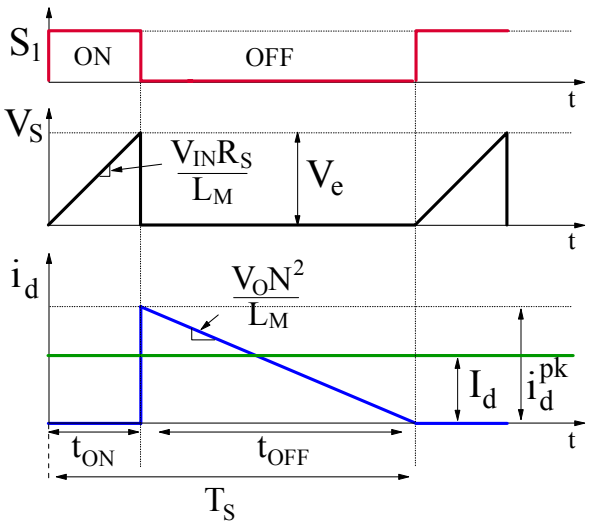

Figure 2. Key switching waveforms of variable-frequency flyback converter.

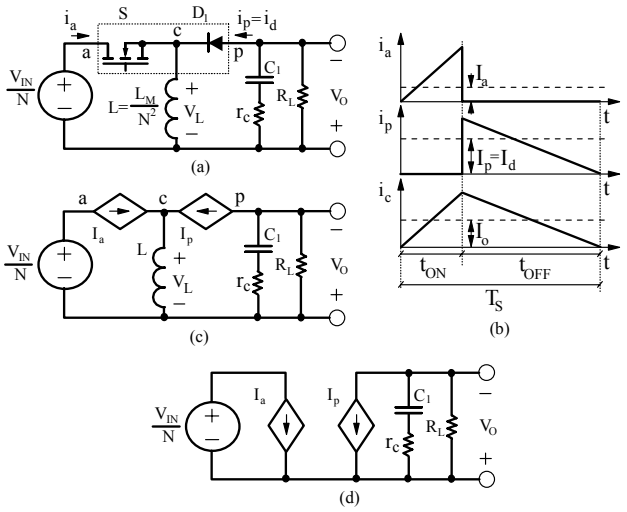

Figure 3. Synthesis of large-signal model; (a) flyback converter reduced to buck-boost converter, (b) key switching waveforms, (c) large-signal model, (d) large-signal model neglecting inductance L.

where sources I_a and I_p represent the average values of terminal currents i_a and i_p over a switching cycle, as shown in Fig. 3(c). Due to boundary operation, the converter shown in Fig. 1 delivers the entire magnetizing energy stored during on time t_{ON} to the output during off time t_{OFF}. Moreover, since the converter operates at the boundary of CCM and DCM under any steady state or transient condition, the average inductor voltage is equal to zero (i.e., $\langle v_L \rangle = 0$). As a result, inductor L can be removed from the large-signal model and replaced with a short, as shown in Fig. 3(d), which significantly simplifies the derivation of small-signal transfer function.

The average of passive terminal current i_p over a switching cycle can be expressed as a function of input and output voltages, as well as magnetizing inductance L_M, through duty cycle D and peak diode current i_d^{pk},

$$I_p = I_d = i_d^{pk}(1-D)/2 = \frac{V_{IN} t_{ON} N}{2L_M}\left(1 - 1\Big/\left(\frac{1}{M \cdot N} + 1\right)\right), \quad (1)$$

where $i_d^{pk} = V_{IN} t_{ON} N / L_M$, $M = (V_O + V_F)/V_{IN}$, duty cycle $D = 1/\left(1 + (M \cdot N)^{-1}\right)$, and V_F is the forward voltage drop across output diode D_1. On time t_{ON} can be related to error voltage V_e, as shown in Fig. 2,

$$t_{ON} = V_e L_M / (V_{IN} R_S). \quad (2)$$

Substituting (2) into (1),

$$I_d = \frac{V_e}{2R_S} \frac{N}{1 + N(V_O + V_F)/V_{IN}}. \quad (3)$$

Equation 3 shows that current I_d is nonlinearly dependent on input voltage V_{IN}, output voltage V_O, and error voltage V_e. Unlike conventional PWM converters, whose control variable is the duty cycle of the main switch, DCM/CCM boundary mode converters control the output voltage by varying the on time of the main switch, which, in turn, controls average diode

current I_d. As a result, duty cycle D remains nearly constant. Output voltage V_O is established by average diode current I_d and the impedance of the filter and load (i.e., $V_O = I_d Z$, where impedance Z is equal to the parallel connection of the load and filter capacitor C_1, as shown in Fig. 4).

B. *Small-Signal Model*

The small signal model can be obtained from Fig. 3(d) by setting all dc voltage sources to zero (i.e., replacing with a short circuit) and by removing all dc current sources (i.e., replacing with open circuit). From (3), current I_d is then linearized around its steady state operating point ,

$$\hat{I}_d = I_d(V_e, V_{IN}, V_O) = K_e \hat{V}_e + K_f \hat{V}_{IN} + K_r \hat{V}_O , \qquad (4)$$

where $K_e = \partial I_d / \partial V_e$, $K_f = \partial I_d / \partial V_{IN}$, and $K_r = \partial I_d / \partial V_O$, all of which are summarized in Table 1. It should be noted that each partial derivative in Table 1 is written as a function of V_e, V_O, and V_{IN} steady-state values. Equation (4) can be represented by a circuit diagram along with the output filter, as illustrated in Fig. 4.

From Fig. 4, the average diode current I_d develops output voltage V_O across impedance Z, where

$$Z = \frac{\hat{V}_O}{\hat{I}_d} = \frac{R_L(1 + sC_1 r_c)}{1 + sC_1(r_c + R_L)} , \qquad (5)$$

and

$$\hat{V}_O = \hat{I}_d Z = Z(K_e \hat{V}_e + K_r \hat{V}_O + K_f \hat{V}_{IN}) . \qquad (6)$$

From (6), control-to-output transfer function G_{VC} is determined as

$$G_{VC} = \left.\frac{\hat{V}_O}{\hat{V}_e}\right|_{\hat{V}_{IN}=0} = \frac{ZK_e}{1 - ZK_r} . \qquad (7)$$

Rearranging into pole-zero form,

$$G_{VC} = \frac{K_e}{-K_r + 1/R_L} \frac{1 + s/\omega_{zc}}{1 + s/\omega_{p1}} , \qquad (8)$$

where K_e, K_r, ω_{zc}, and ω_{p1} are given in Table 1. Very often, a constant-current load is used in place of a constant resistance load for worst-case evaluation since it offers the least amount of damping (i.e., high Q). In this case, resistance R_L is replaced with a dc current sink in the large signal model, and, therefore, is replaced with an open circuit (i.e., $R_L \rightarrow \infty$) in both the small-signal circuit diagram and in (8).

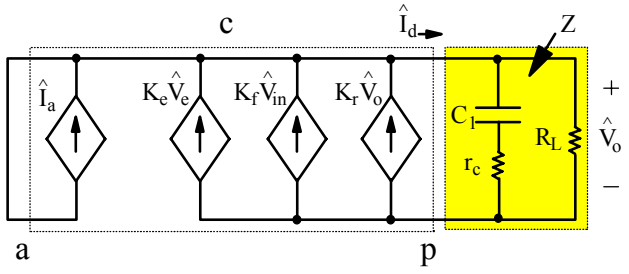

Figure 4. Small-signal model of variable-frequency flyback converter.

III. RINGING CHOKE CONVERTER

A common implementation of the variable frequency flyback converter is shown in Fig. 5 along with key switching waveforms shown in Fig. 6. This circuit, also referred to as ringing choke converter (RCC), is simple and cost effective since the control is implemented discretely. The control consists of positive feedback winding N_{S2}, error amplifier TL431, and bipolar junction transistor (BJT) Q_1, as well as resistors R_S, R_F, R_A, R_{ST}, and R_{ZCD}, capacitor C_{ZCD}, zener clamp diode ZD_1, and optocoupler IC_1.

Error amplifier cathode-to-anode voltage V_{EA}, which represents the amplified difference between output voltage V_O and the internal voltage reference of TL431, directly controls error amplifier current i_{EA}. Error amplifier current i_{EA} establishes error current i_e through optocoupler IC_1, which develops error voltage V_e across the sum of resistors R_F and R_S, where $V_e = i_e(R_F + R_S)$. Error voltage V_e is summed with sense voltage V_S, where $V_S = i_{S1} R_S$, to form base-emitter voltage V_{Qbe}. While switch S_1 is on, base-emitter voltage V_{Qbe} increases linearly until it reaches cut-off voltage level V_γ of BJT Q_1 (typically around 0.6 V), at which time, BJT Q_1 begins to discharge the input capacitance of main switch S_1 until finally, switch S_1 turns off after discharge time t_C. Magnetizing energy, which was stored in transformer T_1 during switch S_1 on time, is completely delivered to the output while switch S_1 is off, at which time, positive feedback winding N_{S2} polarity changes, initiating turn on of switch S_1 through resistor R_{ZCD} and capacitor C_{ZCD}, completing a switching cycle. Please note that a more detailed analysis of RCC operation is given in [6].

A. *Small-Signal Model of RCC*

The procedure for determining the control-to-output transfer function G_{VC} of the RCC circuit shown in Fig. 5 is

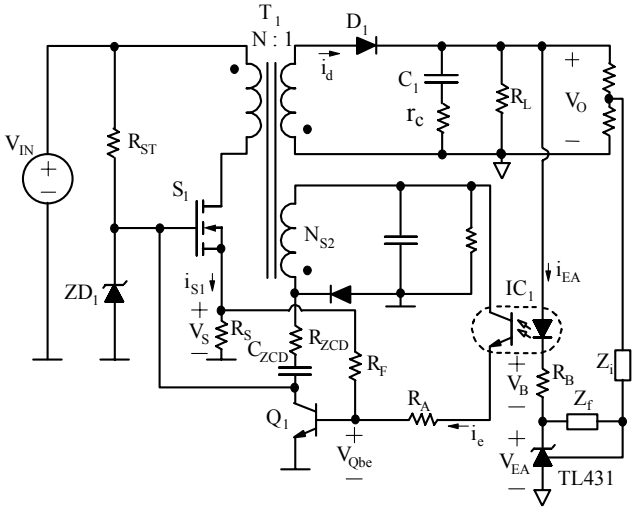

Figure 5. Circuit diagram of ringing-choke converter (RCC).

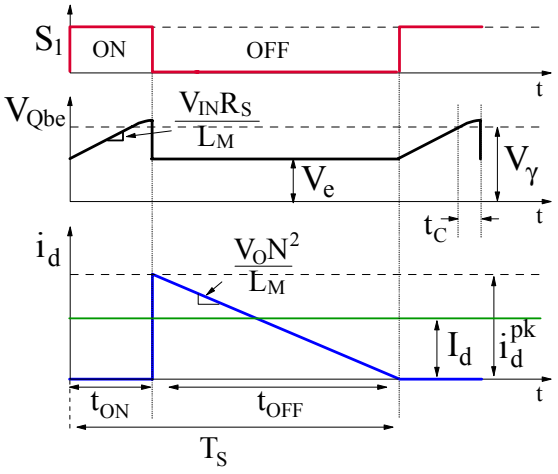

Figure 6. Key switching waveforms of ringing-choke converter (RCC).

identical to that previously discussed for the variable frequency flyback converter. From Fig. 6, on time t_{ON} can be expressed as a function of both error voltage V_e and BJT cut-off voltage V_γ,

$$t_{ON} = \frac{(V_\gamma - V_e)L_M}{V_{IN}} + t_C , \qquad (9)$$

where t_C is the discharge time of input capacitance C_{iss} of main switch S_1. Discharge time t_C can be approximated as

$$t_C \approx \frac{C_{iss}}{2\pi h_{oe}} , \qquad (10)$$

where h_{oe} is the small signal output admittance of BJT Q_1. It should be noted that discharge time t_C is nearly constant over line and load range, and can be omitted without significant loss of accuracy.

Substituting (9) into (1), average diode current I_d is written as a function of error voltage V_e, input voltage V_{IN}, and output voltage V_O,

$$I_d = \frac{N}{2}\left(V_\gamma - V_e + \frac{V_{IN}t_C}{L_M}\right)\left(\frac{1}{1+N(V_O+V_F)/V_{IN}}\right). \qquad (11)$$

As before, average diode current I_d is linearized around its steady state operating point, and expressed as a function of coefficients K_e, K_r, and K_f, as shown in (4) and given in Table 1, where K_e, K_r, and K_f differ from those determined for the variable frequency flyback converter.

The full block diagram of RCC circuit, which was introduced in [6], is shown in Fig. 7. The block diagram consists of control-to-output voltage transfer function $G_{VC}(s) = \hat{V}_O/\hat{V}_e$, output voltage sensing gain $K_d = \hat{V}_1/\hat{V}_O$, error amplifier transfer function $G_{EA}(s) = \hat{V}_{EA}/\hat{V}_1$, transconductance gain $G_1 = \hat{i}_{EA}/\hat{V}_B$, opto-coupler gain $G_2 = \hat{i}_e/\hat{i}_{EA}$, and transresistance gain $G_3 = \hat{V}_e/\hat{i}_e$.

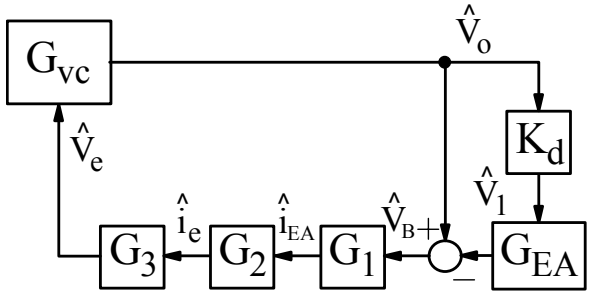

Figure 7. Small-signal block diagram of ringing-choke converter (RCC).

B. *Validation of Small-Signal Model of RCC*

An offline, 5-V/ 2-A RCC converter with constant resistance type load was used to validate the model. Since error voltage V_e is generally not accessible, measurements were taken from error current i_e to output voltage V_O, which can be related back to control-to-output transfer function G_{VC} through gain G_3,

$$\frac{\hat{V}_O}{\hat{i}_e} = G_{VC}G_3 = G_{VC}(R_F + R_S) , \qquad (12)$$

where $G_3 = R_F + R_S$. As can be seen from Fig. 8, agreement between calculated and measured results is excellent for the gain, and moderately good for the phase, up to one tenth of switching frequency f_S (i.e., up to 4 kHz). Above one tenth of switching frequency f_S, the measured phase diverges from the calculated phase. This is likely due to the sampling gain, which was first introduced by [7], since the peaking occurs at harmonics of the switching frequency accompanied by a significant drop in phase. Note that the phase begins at approximately –180 degrees since the dc gain is negative. In fact, control-to-output transfer function G_{VC} contains the inversion necessary to achieve negative feedback in the RCC circuit shown in Fig. 5. It has been suggested in [3] and [4] that an RHP zero is present in control-to-output transfer function G_{VC}. However in the case of our offline RCC prototype circuit, according to the equation given in [3] and [4], the location of RHP zero would be well above the switching frequency.

C. *Small-Signal Model of RCC with Second-Stage LC Filter*

In order to better attenuate the switching ripple at the output without significantly impacting the filter cost and volume, an additional LC output filter stage is often used as an alternative to simply paralleling more output capacitors, as shown in Fig. 9. The addition of a second stage LC filter changes the dynamics of control-to-output transfer function G_{VC}, and increases the order of the characteristic polynomial. Since it is very cumbersome to derive an expression for the roots of a polynomial greater than second order, designers often resort to a cut-and-try approach when compensating the control loop. However, in the case of variable frequency flyback converter with second stage LC filter, the roots of the characteristic polynomial are obtainable, with an approximation, since it can be modeled as a third order system.

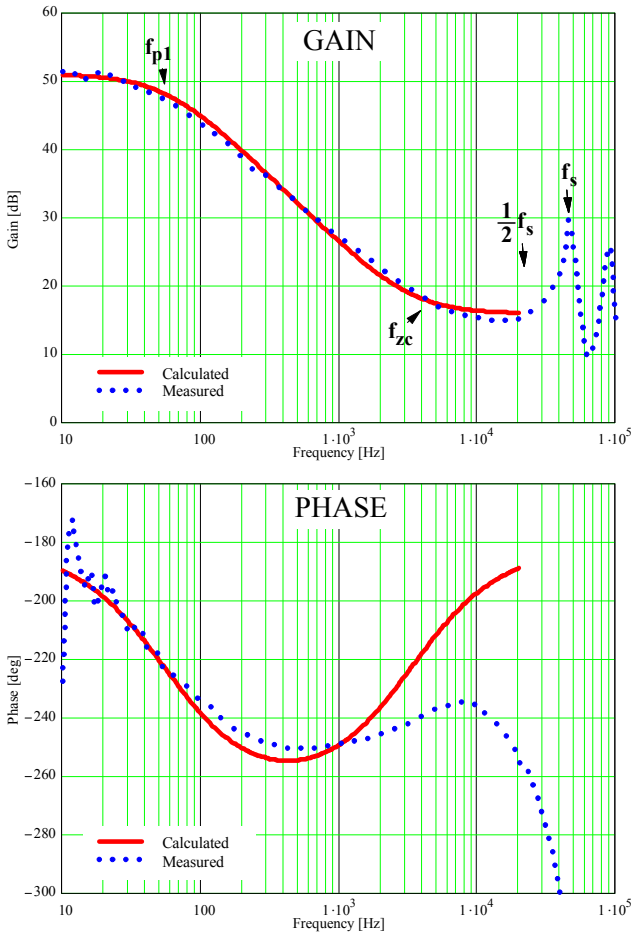

Figure 8. Calculated and measured Bode plots of control-to-output stage transfer function of RCC. Parameters: V_{IN}=315 V, N=17.2, R_S=1.5Ω, L_M=4mH, R_L=2.5Ω, C_1=1.4mF, r_c=35mΩ, R_F=39Ω, t_C=1μs, f_S=45 kHz, f_{p1}=57 Hz, f_{zc}=3.2 kHz

Since the average voltage across filter inductor L_f is zero (neglecting its equivalent series resistance) under steady state operation, impedance Z of (6) and (7) can be replaced with

$$Z = \frac{\hat{V}_O}{\hat{I}_d} = \frac{Z_1 Z_3}{Z_1 + Z_2 + Z_3}, \qquad (13)$$

where $Z_1 = (sC_{f1}r_{cf1}+1)/sC_{f1}$, $Z_2 = sL_f$, and $Z_3 = R_L(sC_{f2}r_{cf2}+1)/(sC_{f2}(r_{cf2}+R_L)+1)$, as shown in Fig. 10. Typically, a small filter inductance (e.g. L_f < 15uH) is usually sufficient to provide adequate attenuation of switching ripple, and, therefore, the roots of the third order characteristic polynomial are determined with the approximation that at low frequencies (i.e., at frequencies below desired loop crossover frequency), the impedance of Z_2 is negligible with respect to Z_1 and Z_3. The filter then appears as two capacitors connected in parallel, where the equivalent capacitance is approximately their sum, (i.e., $C_1 = C_{f1} + C_{f2}$) and equivalent series resistance is approximately their reciprocal sum ($r_c = r_{cf1} // r_{cf2}$). The first, low-frequency pole ω_{p1} is identified as before, and is extracted

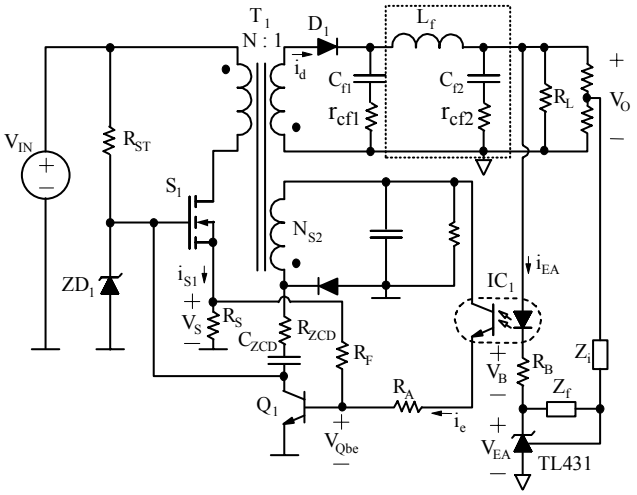

Figure 9. Circuit diagram of ringing-choke converter with second-stage LC filter.

from the third order polynomial, leaving a second order polynomial. After considerable algebraic manipulation, and applying the approximation that equivalent series resistances r_{cf1} and r_{cf2} are much less than output resistance R_L, i.e., $r_{cf1} << R_L$ and $r_{cf2} << R_L$, control-to-output transfer function G_{VC} can be written in pole-zero form,

$$G_{VC}(s) = \frac{\hat{V}_O}{\hat{V}_e} = \frac{K_e}{-K_r + 1/R_L} \frac{(1+s/\omega_{zc1})(1+s/\omega_{zc2})}{(1+s/s_{p1})\left(1+\frac{s}{Q\omega_O}+\frac{s^2}{\omega_O^2}\right)}, \qquad (14)$$

where filter zeros ω_{zc1} and ω_{zc2}, as well as resonant pole ω_O and quality factor Q, are given in Table 1. Note that the expression in (14) is equivalent to those presented previously [6].

D. Validation of Small-Signal Model of RCC with Second-Stage LC Filter

A second stage LC filter was added to the output of an offline, 5-V/ 2-A RCC converter with a constant-resistance load, and a comparison between measured and calculated results is shown in Fig. 11. As before, there is excellent agreement up to one-tenth of the switching frequency in both the phase and the gain. Above one-tenth of the switching frequency, the measured phase diverges from the calculated phase.

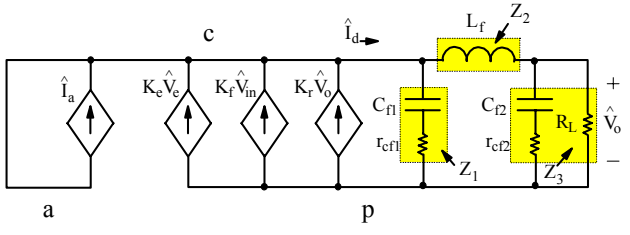

Figure 10. Small-signal model of variable-frequency converter with second stage LC filter.

TABLE I. SMALL-SIGNAL TRANSFER FUNCTION GAIN, POLE, AND ZERO LOCATIONS

	VARIABLE FREQUENCY FLYBACK	RINGING CHOKE CONVERTER
K_e	$\frac{N}{2R_S}\frac{1}{1+NM}$	$-\frac{N}{2R_S}\frac{1}{1+NM}$
K_r	$-\frac{N^2V_e}{2R_S}\frac{1}{V_{IN}(1+NM)^2}$	$-\frac{N^2}{2}\frac{\left(\frac{V_\gamma - V_e}{R_S}+V_{IN}\frac{t_C}{L_M}\right)}{V_{IN}(1+NM)^2}$
K_f	$\frac{N^2V_oV_e}{2V_{IN}^2R_S}\frac{1}{(1+NM)^2}$	$\frac{Nt_C}{2L_M(1+NM)}+\frac{N^2M\left(\frac{V_\gamma - V_e}{R_S}+V_{IN}\frac{t_C}{L_M}\right)}{2V_{IN}(1+NM)^2}$
V_e	$\frac{2R_SP_O(1+NM)}{\eta(V_O+V_F)N}$	$V_\gamma-\frac{2R_SP_O(1+MN)}{\eta(V_O+V_F)N}+\frac{V_{IN}R_S}{L_M}t_C$

$$\omega_{p1}=\frac{-K_r+1/R_L}{C_1\left(r_C\left(-K_r+1/R_L\right)+1\right)} \qquad \omega_{zc}=\frac{1}{C_1r_C} \qquad \omega_{zc1}=\frac{1}{C_{f1}r_{Cf1}} \qquad \omega_{zc2}=\frac{1}{C_{f2}r_{Cf2}}$$

$$\omega_o=\sqrt{\frac{1-\left(r_{cf1}\|r_{cf2}\right)K_r}{L_f\left(\frac{C_{f1}C_{f2}}{C_{f1}+C_{f2}}\right)}} \qquad Q=\frac{\omega_o}{\frac{r_{cf1}+r_{cf2}}{L_F}\left(1+\left(r_{cf1}\|r_{cf2}\right)K_r\right)+\frac{1}{C_{f2}R_L}+\frac{K_r-1/R_L}{\left(C_{f1}+C_{f2}\right)\left(1-\left(r_{cf1}\|r_{cf2}\right)K_r\right)}}$$

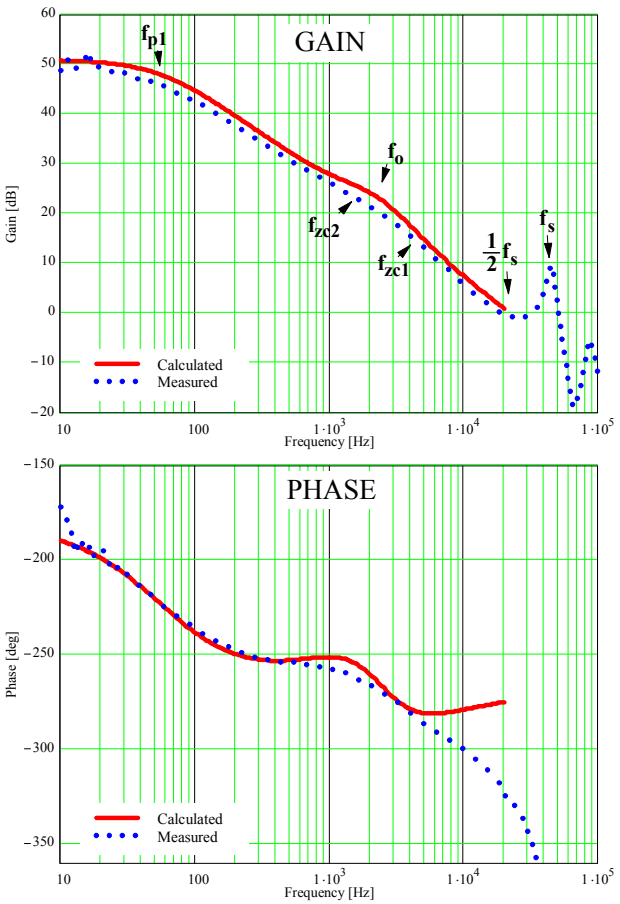

Figure 11. Calculated and measured Bode plots of control-to-output transfer function of RCC with second stage LC filter. Parameters: V_{IN}=315 V, N=17.2, R_S=1.5Ω, L_M=4mH, R_L=2.5Ω, C_{f1}=1mF, C_{f2}=470μF r_{cf1}=0.04Ω, r_{cf2}=0.27Ω, L_f=14μF, R_F=39Ω, t_C=1μs, f_S=45 kHz, f_{p1}=57 Hz, f_{zc1}=4kHz, f_{zc2}=1.3kHz, f_O=2.4kHz

IV. SUMMARY

A simple small-signal model for variable frequency flyback converter which operates at the boundary of DCM/CCM with current mode control was developed. The model was validated on an offline, 5-V/ 2-A experimental prototype and was shown to have excellent agreement in both gain and phase up to one-tenth of the switching frequency.

REFERENCES

[1] R.B. Ridley, "A new continuous-time model for current-mode control with constant frequency, constant on-time, and constant off-time, in ccm and dcm", IEEE Power Electronics Specialists Conf. (PESC) Rec., pp.382-389, June 1990.

[2] V.Vorperian, "Simplified analysis of pwm converters using the model of the pwm switch part II: discontinuous conduction mode", Virginia Power Electronics Center (VPEC) Seminar Proc., pp.10-20, Sept. 1989.

[3] J. Lempinen and T. Suntio, "Small-signal modeling for design of robust variable-frequency flyback battery chargers for portable device applications", IEEE Applied Power Electronics Conf. (APEC) Proc., pp.548-554, March 2001.

[4] J. Chen, R. Erickson, and D. Maksimović, "Averaged switch modeling of boundary conduction mode dc-to-dc converters", IEEE Industrial Electronics Society Conf. (IECON), pp.844-849, Nov. 2001.

[5] D.M. Mitchell, "Tricks of the trade: understanding the right-half-plane zero in small-signal dc-dc converter models", IEEE Power Electronics Society Newsletter, pp.5-6, January 2001.

[6] B.T. Irving and M.M. Jovanović, "Analysis and design of self-oscillating flyback converter", IEEE Applied Power Electronics Conf. (APEC) Proc., pp.897-903, March 2002.

[7] R.B. Ridley, "A new small-signal model for current-mode control", PhD Dissertation, Virgina Polytechnic Institute and State University, Blacksburg, VA, 1990.